

PSFC/JA-03-05

**Asymptotic analysis of dispersion
characteristics in two-dimensional
metallic photonic band gap structures**

Evgenya I. Smirnova and Chipping Chen

February 2003

Plasma Science and Fusion Center
Massachusetts Institute of Technology
Cambridge, MA 02139 USA

This work was supported in part by the Innovative Vacuum Electronics MURI Program, in part by the Department of Energy, High Energy Physics Division, and in part by Tech-X Corporation. Reproduction, translation, publication, use and disposal, in whole or in part, by or for the United States government is permitted.

Submitted for publication to *Journal of Applied Physics*.

ASYMPTOTIC ANALYSIS OF DISPERSION CHARACTERISTICS IN TWO-DIMENSIONAL METALLIC PHOTONIC BAND GAP STRUCTURES

Evgenya I. Smirnova and Chiping Chen
Plasma Science and Fusion Center
Massachusetts Institute of Technology
Cambridge, Massachusetts 02139

We present a self-consistent technique for the asymptotic analysis of dispersion curves in two-dimensional (2D) metallic photonic band gap (PBG) structures representing square and triangular arrays of metal rods. The technique is applicable for the structures with rod radii (a), which are small compared to the distance between the rods (b) and to the wavelength (λ). The induced current and charge distributions on the rods are expressed self-consistently in terms of the electromagnetic wave field. The dispersion characteristics are calculated for the TE and TM modes. The results are in agreement with those obtained previously using the Photonic Band Gap Structure Simulator (PBGSS) code.

42.70. Qs, 41.20.Jb

I. INTRODUCTION

Photonic band gap (PBG) structures [1] provide exciting new ways to control electromagnetic waves in optical [2,3] and microwave devices [4-7]. In particular, they can be successfully applied for higher order mode (wakefields) suppression in microwave linear accelerators. The wakefields are unwanted modes, which are excited by an interaction of an intense electron beam with the rf circuit. They can affect the propagation of other electron beams. To obtain high-efficiency acceleration, the acceleration cavities must be selective with respect to the operating mode, while suppressing unwanted oscillations. Use of the two-dimensional (2D) metallic PBG structures has been shown experimentally to be a promising approach to the realization of such mode selective circuits [4-7].

A PBG structure (photonic crystal) represents a lattice of macroscopic pieces (for example, rods or spheres) of dielectric or metal. One can design photonic crystals with photonic band gaps, preventing light of certain frequencies from propagating in certain directions. If, for some frequency range, a photonic crystal reflects light incident at any angle, the crystal has a global photonic band gap. Calculation of the fundamental and higher frequency global photonic band gaps is an important problem. To solve this problem for metallic lattices, a computer code, called the Photonic Band Gap Structure Simulator (PBGSS), was developed recently at Massachusetts Institute of Technology [8]. However the finite difference method employed for the calculation of the dispersion characteristics in Ref. [8] was unable to reveal the nature of the wave interactions in PBG structures. In this paper we present an asymptotic analysis, which allows us to study these interactions and improves our understanding of the physics.

We study TM and TE modes propagating in square and triangular lattices of metal rods (see Fig. 1). We consider the limit when the rod radius, a , is much smaller than the wavelength $\lambda = 2\pi/k_{\perp}$ and the distance between the rods, b . In this limit we can separate two regions in the 2D lattice with the qualitatively different behavior of electromagnetic waves. The *near-field* region is the one that immediately surrounds the rod. In this region the field changes at the scale of the rod radius and we can apply an approximate (quasistatic [9]) approach to calculate self-consistently the sources (charges and currents) in the metallic rods due to the electromagnetic waves in the lattice. The region beyond the near-field region is the *far-field* region, where the field changes at the scale of the wavelength. According to Bloch's theorem, the electromagnetic field in the lattice can be decomposed into a set of plane waves with the wave vectors multiple of

the reciprocal lattice vectors. The currents, calculated self-consistently in the near-field region, are shown to produce the coupling of several plane waves at the metal rods. The coupling perturbs the plane-wave dispersion relations in the lattice and produces the dispersion characteristics, which are different for the TM and TE waves. Thus, the form of the dispersion curves is determined by both, the lattice symmetries, and the plane-wave coupling at the metal rods.

The results of the quasistatic calculation of the TM and TE dispersion characteristics are presented. We compare the results of the quasistatic calculation to those obtained previously using the PBGSS code [8]. A good agreement is found.

The quasistatic method in 2D metallic lattices may be generalized to treat 2D the dielectric lattices and dielectric-metallic hybrids [10]. Moreover, three-dimensional PBG structures [1] such as dielectric or metallic lattices or dielectric-metallic hybrids may be studied with this technique. Finally, the self-consistent expressions for the currents in the rods allow the calculation of modes localized around the defects in lattices, such as those studied in [4-7, 11, 12].

The article is organized as follows. In Sec. II, we discuss the symmetries of 2D lattices and present a general description of electromagnetic waves in periodic structures. In Sec. III, we formulate the basis of the quasistatic approach, calculate self-consistently the currents in the metal rods due to the electromagnetic fields, and derive the dispersion characteristics for the TM and TE waves. We illustrate the physics of plane-wave interactions with several examples. Conclusions are presented in Sec. IV.

II. ELECTROMAGNETIC WAVE PROPAGATION IN PBG STRUCTURES

We consider two lattices of long perfectly conducting rods, namely, the square lattice [Fig. 1(a)] and the triangular lattice [Fig. 1(b)], which were studied in Ref.⁸. The conductivity profile in the lattices satisfies the periodic condition

$$\sigma(\mathbf{x}_\perp + \mathbf{T}_{m,n}) = \sigma(\mathbf{x}_\perp), \quad (1)$$

with the set of periodicity vectors $\mathbf{T}_{m,n}$ defined as

$$\mathbf{T}_{m,n} = \begin{cases} mb\hat{\mathbf{e}}_x + nb\hat{\mathbf{e}}_y & \text{(square lattice),} \\ \left(m + \frac{n}{2}\right)b\hat{\mathbf{e}}_x + \frac{\sqrt{3}}{2}nb\hat{\mathbf{e}}_y & \text{(triangular lattice).} \end{cases} \quad (2)$$

In Eqs. (1) and (2), $\mathbf{x}_\perp = x\hat{\mathbf{e}}_x + y\hat{\mathbf{e}}_y$ is the transverse coordinate, b is the lattice spacing, and m and n are integers. It is readily shown from Maxwell's equations that the wave field in the two-dimensional PBG structures can be decomposed into two independent sets of modes: transverse electric (TE) modes and transverse magnetic (TM) modes. In a TE (TM) mode the electric (magnetic) field vector is perpendicular to the rod axis (i.e., z -axis). All the field components in the TM (TE) modes can be expressed in terms of the axial component of the electric (magnetic) field, which is further denoted by Ψ . Since the system is homogeneous along the z -axis, we can use the Fourier transform in both the axial coordinate z and time t and consider

$$\psi(\mathbf{x}_\perp, k_z, \omega) = \iint \Psi(\mathbf{x}_\perp, z, t) e^{i(k_z z - \omega t)} dz dt. \quad (3)$$

For simplicity we will use the notation $\psi(\mathbf{x}_\perp)$ instead of $\psi(\mathbf{x}_\perp, k_z, \omega)$ assuming that both frequency ω and longitudinal wave number k_z are fixed. The Helmholtz equation for the wave function $\psi(\mathbf{x}_\perp)$ follows from the Maxwell equations,

$$\nabla_\perp^2 \psi(\mathbf{x}_\perp) = \left(k_z^2 - \frac{\omega^2}{c^2} \right) \psi(\mathbf{x}_\perp), \quad (4)$$

and is valid for $|\mathbf{x}_\perp - \mathbf{T}_{m,n}| > a$ in every unit cell of the lattice.

Let $\rho(\mathbf{x}_\perp, k_z, \omega)$ and $\mathbf{J}(\mathbf{x}_\perp, k_z, \omega)$ be the charge and current densities induced by the field at the surfaces of the conducting rods. The Helmholtz equation (4) can be generalized for the entire space (vacuum and conducting rods), if the charges and currents are included. The generalized Helmholtz equation is

$$\nabla_\perp^2 \psi(\mathbf{x}_\perp) + \kappa^2 \psi(\mathbf{x}_\perp) = f(\mathbf{x}_\perp), \quad (5)$$

where $\kappa^2 = \omega^2 / c^2 - k_z^2$, and $f(\mathbf{x}_\perp)$ is a function, related to the currents and charges

$$f(\mathbf{x}_\perp) = \begin{cases} i4\pi k_z \rho(\mathbf{x}_\perp) - \frac{i4\pi\omega}{c^2} J_z(\mathbf{x}_\perp) & \text{(TM case),} \\ -4\pi \left(\frac{1}{c} \nabla \times \mathbf{J} \right)_z & \text{(TE case).} \end{cases} \quad (6)$$

Bloch's theorem allows us to expand $\psi(\mathbf{x}_\perp)$ in a Fourier series,

$$\psi(\mathbf{x}_\perp) = e^{i\mathbf{k}_\perp \cdot \mathbf{x}_\perp} \sum_{m,n} \psi_{m,n} e^{i\mathbf{G}_{m,n} \cdot \mathbf{x}_\perp} \quad (7)$$

with \mathbf{k}_\perp being an arbitrary wave vector perpendicular to the rods and $\mathbf{G}_{m,n}$ being vectors of the reciprocal lattice [13]. Reciprocal lattice vectors are related to $\mathbf{T}_{m,n}$ by the orthogonality condition $\mathbf{G}_{m,n} \cdot \mathbf{T}_{m',n'} = 2\pi\delta_{m,m'}\delta_{n,n'}$. This yields

$$\mathbf{G}_{m,n} = \begin{cases} \frac{2\pi}{b} (\hat{\mathbf{e}}_x m + \hat{\mathbf{e}}_y n) & \text{(square lattice),} \\ \frac{2\pi}{b} \left[\left(\hat{\mathbf{e}}_x - \frac{1}{\sqrt{3}} \hat{\mathbf{e}}_y \right) m + \frac{2}{\sqrt{3}} \hat{\mathbf{e}}_y n \right] & \text{(triangular lattice).} \end{cases} \quad (8)$$

Physically, the Fourier series in Eq. (7) corresponds to an expansion of the electromagnetic field into a set of orthogonal plane waves. Only the plane waves with certain wave numbers can exist in the periodic lattice. With the aid of Eq. (7), Eq. (5) can be rewritten as

$$\sum_{m,n} \left[\kappa^2 - (\mathbf{k}_\perp + \mathbf{G}_{m,n})^2 \right] \psi_{m,n} e^{i\mathbf{k}_\perp \cdot \mathbf{x}_\perp + i\mathbf{G}_{m,n} \cdot \mathbf{x}_\perp} = f(\mathbf{x}_\perp). \quad (9)$$

Multiplying Eq. (9) by $e^{-i\mathbf{k}_\perp \cdot \mathbf{x}_\perp - i\mathbf{G}_{m,n} \cdot \mathbf{x}_\perp}$ and integrating over the elementary cell area, A , yields

$$\left[\kappa^2 - (\mathbf{k}_\perp + \mathbf{G}_{m,n})^2 \right] \psi_{m,n} = \frac{1}{A} \int_{el.cell} f(\mathbf{x}_\perp) e^{-i\mathbf{k}_\perp \cdot \mathbf{x}_\perp - i\mathbf{G}_{m,n} \cdot \mathbf{x}_\perp} d^2 \mathbf{x}_\perp. \quad (10)$$

The simplest approximation to solve the system of equations (10) can be made using the assumption that there is no interaction between the rods and the electromagnetic waves, i.e., $f(\mathbf{x}_\perp) = 0$. This is called the "plane-wave approximation" [2,14]. The eigenfrequencies obtained in the framework of this approximation are simply

$$\left(\frac{\omega}{c} \right)_{m,n} = |\mathbf{k}_\perp + \mathbf{G}_{m,n}|. \quad (11)$$

The dispersion curves given by Eq. (11) are the consequence of only the crystal symmetries. They are independent of the nature of the interactions in the periodic structure and are the same for all photonic crystals with the same geometry. The dispersion curves in the plane-wave approximation for both the square and triangular lattices are plotted in Ref. [14].

III. QUASISTATIC APPROXIMATION FOR THIN CONDUCTING RODS

The plane-wave approximation discussed at the end of Sec. II is a zeroth-order analysis. In this section, we consider a first-order approximation for $f(\mathbf{x}_\perp)$, which describes the interactions between the electromagnetic waves and conducting rods in Eqs. (10). The first-order approximation holds in the limit when the rods are small compared to the wavelength, i.e., $\kappa a \ll 1$ (quasistatic limit) and to the distance between the rods, i.e., $a/b \ll 1$. In this limit, approximations can be made to the wave equation (5), and the source $f(\mathbf{x}_\perp)$ can be self-consistently related to the wave function $\psi(\mathbf{x}_\perp)$.

Assume that the center of the rod (m, n) is located at $\mathbf{x}_\perp = \mathbf{T}_{m,n}$. There are two regions surrounding the rod (m, n) , where the behavior of $\psi^{(m,n)}(\mathbf{x}_\perp)$ is qualitatively different [15]: *near-field* region and *far-field* region, as shown in Fig. 2. We introduce the notation $\mathbf{r} = \mathbf{x}_\perp - \mathbf{T}_{m,n}$. In the *near-field* region where $\kappa r \ll 1$, the wave function $\psi^{(m,n)}$ changes rapidly, i.e.,

$$|\nabla^2 \psi_{near}^{(m,n)}| \sim \psi_{near}^{(m,n)} / a^2 \gg \kappa^2 \psi_{near}^{(m,n)}. \quad (12)$$

In the *far-field* region where $\kappa r \geq 1$, the wave-function $\psi^{(m,n)}$ changes slowly, i.e.,

$$|\nabla^2 \psi_{far}^{(m,n)}| \sim \kappa^2 \psi_{far}^{(m,n)}. \quad (13)$$

The near- and the far-field solutions must match at the boundary of the two regions,

$$\psi_{near}^{(m,n)} \Big|_{r \sim 1/\kappa} = \psi_{far}^{(m,n)} \Big|_{r \sim 1/\kappa}. \quad (14)$$

In the remainder of this section, we use the near- and the far-field solutions to derive approximate self-consistent expressions for the sources $f(\mathbf{x}_\perp)$ and solve the system of Eqs. (10).

We now consider the TM and TE modes separately.

A. TM case

Outside the conducting rods we have $f(\mathbf{x}_\perp) = 0$. Taking into account Eq. (12), we write Eq. (5) in the near-field region in the electrostatic approximation as

$$\nabla^2 \psi_{near}^{(m,n)} = 0. \quad (15)$$

For the TM case the boundary condition at the rod is given by

$$\psi_{near}^{(m,n)} \Big|_{r=a} = 0. \quad (16)$$

The general solution of the Laplace Eq. (15) in 2D is given by

$$\psi_{near}^{(m,n)} = a_0 + b_0 \ln r + \sum_{l=1}^{\infty} \left(a_l r^l + \frac{b_l}{r^l} \right) [p_l \cos(l\theta) + q_l \sin(l\theta)]. \quad (17)$$

Here a_l, b_l, p_l, q_l are arbitrary constants. It is sufficient to keep only the first two terms in Eq. (17) to be able to satisfy the boundary conditions in Eqs. (14) and (16). The solution satisfying the boundary conditions is

$$\psi_{near}^{(m,n)} = \psi_{far}^{(m,n)} \left[1 - \frac{\ln(\kappa r)}{\ln(\kappa a)} \right]. \quad (18)$$

Using the solution in Eq. (18) we can calculate the source in the rod (m, n) creating this field. We obtain

$$f^{(m,n)}(\mathbf{r}) = \nabla_{\perp}^2 \psi_{near}^{(m,n)} \cong -\frac{\psi_{far}^{(m,n)}}{\ln(\kappa a)} \nabla_{\perp}^2 \ln(\kappa r) = -\frac{2\pi}{\ln(\kappa a)} \psi_{far}^{(m,n)} \delta(\mathbf{r}). \quad (19)$$

Here $f^{(m,n)}(\mathbf{r})$ is the source in the rod (m, n) . In the vicinity of the rod (m, n) with the source in a single rod included the equation for ψ becomes

$$\nabla_{\perp}^2 \psi + \kappa^2 \psi = -\frac{2\pi}{\ln(\kappa a)} \psi_{far}^{(m,n)} \delta(\mathbf{r}). \quad (20)$$

The far-field solutions of different rods must match: $\psi_{far}^{(m,n)} \equiv \psi(\mathbf{x}_{\perp})$. For a periodic system of conducting rods, we must sum over all the rods to calculate the total sources and obtain the following wave equation:

$$\begin{aligned} \nabla_{\perp}^2 \psi(\mathbf{x}_{\perp}) + \kappa^2 \psi(\mathbf{x}_{\perp}) &= f(\mathbf{x}_{\perp}) = -\frac{2\pi}{\ln(\kappa a)} \sum_{m,n} \psi_{far}^{(m,n)} \delta(\mathbf{x}_{\perp} - \mathbf{T}_{m,n}) \\ &= -\frac{2\pi}{\ln(\kappa a)} \sum_{m,n} \psi(\mathbf{x}_{\perp}) \delta(\mathbf{x}_{\perp} - \mathbf{T}_{m,n}). \end{aligned} \quad (21)$$

Equation (10) along with $f(\mathbf{x}_{\perp})$ from Eq. (21) becomes

$$\left[\kappa^2 - (\mathbf{k}_{\perp} + \mathbf{G}_{m,n})^2 \right] \psi_{m,n} = -\frac{2\pi}{A \ln(\kappa a)} \sum_{m',n'} \psi_{m',n'}. \quad (22)$$

The eigenvalues κ of the linear system in Eqs. (22) can now be found by diagonalizing the infinite matrix

$$M = \begin{pmatrix} \mathbf{k}_\perp^2 - \frac{\alpha}{A} & -\frac{\alpha}{A} & \dots & -\frac{\alpha}{A} & \dots \\ -\frac{\alpha}{A} & (\mathbf{k}_\perp + \mathbf{G}_{0,1})^2 - \frac{\alpha}{A} & \dots & -\frac{\alpha}{A} & \dots \\ \dots & \dots & \dots & \dots & \dots \\ -\frac{\alpha}{A} & -\frac{\alpha}{A} & \dots & (\mathbf{k}_\perp + \mathbf{G}_{m,n})^2 - \frac{\alpha}{A} & \dots \\ \dots & \dots & \dots & \dots & \dots \end{pmatrix}, \quad (23)$$

where $\alpha = \frac{2\pi}{\ln(\kappa a)}$. Because the coefficient α depends on the eigenfrequency κ , the matrix M must be diagonalized iteratively for each eigenvalue.

The eigenvalues of the infinite matrix M can be calculated approximately as the eigenvalues of a truncated matrix with a finite rank. This corresponds to approximating ψ with a finite number of lowest terms of the Fourier representation in Eq. (7). The number of Fourier harmonics in the representation needed to achieve the desired accuracy for κ increases with increasing a/b .

For small a/b the truncation of the Fourier representation in Eq. (7) gives a simple physical picture of the interactions of a finite number of plane waves at the conducting rods of the lattice. For $a/b \rightarrow 0$ the interactions basically become binary, that is, each plane wave interacts primarily with another plane wave, which has the wave vector of the same magnitude. For example, the binary interaction of plane waves can explain the behavior of the lowest local band gap width at the X -points of the square and triangular lattices. We consider the X -point ($\mathbf{k}_\perp = \frac{\pi}{b} \hat{\mathbf{e}}_x$) of the square lattice and restrict ourselves to the interaction of the two plane waves with the lowest values of $|\mathbf{k}_\perp + \mathbf{G}_{m,n}|$. These waves correspond to $(m_1, n_1) = (0, 0)$ and $(m_2, n_2) = (-1, 0)$ with $|\mathbf{k}_\perp + \mathbf{G}_{m,n}| = \frac{\pi}{b}$ for both. The truncated matrix M , describing the interaction of the two waves at the X -point, is simply

$$\tilde{M} = \begin{pmatrix} \frac{\pi^2}{b^2} - \frac{\alpha}{b^2} & -\frac{\alpha}{b^2} \\ -\frac{\alpha}{b^2} & \frac{\pi^2}{b^2} - \frac{\alpha}{b^2} \end{pmatrix}. \quad (24)$$

The eigenvalues of \tilde{M} in Eq. (24) are

$$\begin{aligned}\kappa_1^2 &= \frac{\pi^2}{b^2} \left(1 - \frac{2\alpha}{\pi^2} \right), \\ \kappa_2^2 &= \frac{\pi^2}{b^2}.\end{aligned}\tag{25}$$

Recall that α is a function of κ itself, so the equation for κ_1 must be solved iteratively. To the lowest order, $\alpha \cong \alpha_0 = \frac{2\pi}{\ln(\pi a/b)}$, and the full width of the local band gap at the X-point is given

by

$$\Delta\left(\frac{\omega b}{c}\right) = b(\kappa_2 - \kappa_1) = \frac{\alpha_0}{\pi} = \frac{2}{\ln(\pi a/b)}\tag{26}$$

for small a/b . This logarithmic dependence agrees well with the numerical calculations using the PBGSS code⁸.

Similarly, considering the interaction of two lowest plane waves at the X-point of the triangular lattice ($\mathbf{k}_\perp = \frac{2\pi}{\sqrt{3}b}\hat{\mathbf{e}}_y$), we find that the full width of the local band gap at the X-point of the triangular lattice is given by

$$\Delta\left(\frac{\omega b}{c}\right) = \frac{\alpha_0}{\pi} = \frac{2}{\ln(2\pi a/\sqrt{3}b)}\tag{27}$$

for small a/b .

In the same manner, we numerically calculate the entire dispersion characteristics in the square and triangular lattices by including many plane-wave interactions. For $a/b \rightarrow 0$ only a limited number of the plane waves is needed to achieve a good approximation of ψ . It is reasonable to start the iterative process of solving the matrix M with the initial value for κ being its plane-wave value κ_0 in a given point of the \mathbf{k}_\perp -space. As the eigenvalues of $M[a(\kappa_0)]$ are found, the initial guesses for κ are corrected and new α 's are calculated. Then, the matrix M is diagonalized again with new α 's. The iterative process has been performed using a computer. Results of these calculations are summarized in Fig. 3(a) and Fig. 4(a). In Fig. 3(a) the results are shown for the TM mode in a square lattice with $a/b = 0.05$. The quasistatically calculated eigenvalues are plotted with dots. Solid curves show the dispersion characteristics obtained from the PBGSS calculations⁸. Five to twelve lowest vectors of the reciprocal lattice, depending on the symmetry of the particular \mathbf{k} -point, are taken into account, and the four lowest eigenmodes are

plotted. Similarly, in Fig. 4(a), the results are shown for the TM mode in a triangular lattice with $a/b = 0.05$. As in Fig. 3(a), the eigenvalues calculated with the quasistatic approximation are plotted with dots, whereas the solid curves show the dispersion characteristics obtained from the PBGSS calculations⁸. Six to twelve of the lowest vectors of the reciprocal lattice are taken into account, and the four lowest eigenfrequencies are plotted. The three special points in Fig. 3(a), Γ , X, and M, correspond to $\mathbf{k}_\perp = 0$, $\mathbf{k}_\perp = \frac{\pi}{a}\hat{\mathbf{e}}_x$ and $\mathbf{k}_\perp = \frac{\pi}{a}(\hat{\mathbf{e}}_x + \hat{\mathbf{e}}_y)$, respectively. The three special points in Fig. 4(a), Γ , X, and J, correspond to $\mathbf{k}_\perp = 0$, $\mathbf{k}_\perp = \frac{2\pi}{\sqrt{3}a}\hat{\mathbf{e}}_y$ and $\mathbf{k}_\perp = \frac{2\pi}{3a}(\hat{\mathbf{e}}_x + \sqrt{3}\hat{\mathbf{e}}_y)$. As seen in both Fig. 3(a) and Fig. 4(a), there is a good agreement between the PBGSS calculations and the quasistatic approximation.

B. TE case

As in the TM case, the Laplace equation is valid for ψ in a near-field region around the rod (m, n) for the TE wave, i.e.,

$$\nabla^2 \psi_{near}^{(m,n)} = 0. \quad (28)$$

For the TE case ψ stands for the longitudinal component of the magnetic field. The boundary condition for ψ at $r = a$ is

$$\left. \frac{\partial \psi_{near}^{(m,n)}}{\partial r} \right|_{r=a} = 0. \quad (29)$$

It is convenient to rewrite the boundary condition at $\kappa r \sim 1$ given by Eq. (14) in the form

$$\left(\mathbf{r} \cdot \nabla \psi_{near}^{(m,n)} \right) \Big|_{r \sim 1/\kappa} = \left(\mathbf{r} \cdot \nabla \psi_{far}^{(m,n)} \right) \Big|_{r \sim 1/\kappa}. \quad (30)$$

It is sufficient to keep only three terms in the general solution of Laplace's equation given by Eq. (17) in order to satisfy the boundary conditions in Eqs. (29) and (30). The solution satisfying the boundary conditions is

$$\psi_{near}^{(m,n)} = a_0 + \left(\mathbf{r} \cdot \nabla_\perp \psi_{far}^{(m,n)} \right) \left(1 + \frac{a^2}{r^2} \right), \quad (31)$$

where a_0 is a constant, and use was made of the relation

$$|\nabla_{\perp} \psi_{far}^{(m,n)}| \left(r + \frac{a^2}{r} \right) \cos \theta = \left(\mathbf{r} \cdot \nabla_{\perp} \psi_{far}^{(m,n)} \right) \left(1 + \frac{a^2}{r^2} \right).$$

Using the solution in Eq. (30), we can find that the source in the rod (m, n) creating this field is

$$f^{(m,n)}(\mathbf{r}) = \nabla_{\perp}^2 \psi_{near}^{(m,n)}(\mathbf{r}) \cong \left[\mathbf{r} \cdot \nabla_{\perp} \psi_{far}^{(m,n)} \right] \nabla_{\perp}^2 \frac{a^2}{r^2} = 2\pi a^2 \nabla_{\perp} \psi_{far}^{(m,n)} \cdot \nabla_{\perp} \delta(\mathbf{r}). \quad (32)$$

The equation for ψ in the vicinity of the rod (m, n) with the source in a single rod included is

$$\nabla_{\perp}^2 \psi + \kappa^2 \psi = 2\pi a^2 \nabla_{\perp} \psi_{far}^{(m,n)} \cdot \nabla_{\perp} \delta(\mathbf{r}). \quad (33)$$

For a periodic system of conducting rods the far-field solutions of different rods must match: $\psi_{far}^{(m,n)} \equiv \psi(\mathbf{x}_{\perp})$. In equation for $\psi(\mathbf{x}_{\perp})$ we sum over the contributions from all the rods to calculate the total sources. This yields

$$\begin{aligned} \nabla_{\perp}^2 \psi(\mathbf{x}_{\perp}) + \kappa^2 \psi(\mathbf{x}_{\perp}) &= f(\mathbf{x}_{\perp}) = 2\pi a^2 \sum_{m,n} \nabla_{\perp} \psi_{far}^{(m,n)} \cdot \nabla_{\perp} \delta(\mathbf{x}_{\perp} - \mathbf{T}_{m,n}) \\ &= 2\pi a^2 \sum_{m,n} \nabla_{\perp} \psi(\mathbf{x}_{\perp}) \cdot \nabla_{\perp} \delta(\mathbf{x}_{\perp} - \mathbf{T}_{m,n}). \end{aligned} \quad (34)$$

Equation (10) with $f(\mathbf{x}_{\perp})$ as in Eq. (34) becomes

$$\left[\kappa^2 - (\mathbf{k}_{\perp} + \mathbf{G}_{m,n})^2 \right] \psi_{m,n} = -\frac{2\pi a^2}{A} \sum_{m',n'} \psi_{m',n'} (\mathbf{k}_{\perp} + \mathbf{G}_{m',n'}) \cdot (\mathbf{k}_{\perp} + \mathbf{G}_{m,n}). \quad (35)$$

The eigenvalues κ of the system can now be found by diagonalizing the infinite matrix

$$M = \begin{vmatrix} \mathbf{k}_{\perp}^2 & -\alpha(\mathbf{k}_{\perp} + \mathbf{G}_{0,1}) \cdot \mathbf{k}_{\perp} & \cdots & -\alpha(\mathbf{k}_{\perp} + \mathbf{G}_{m,n}) \cdot \mathbf{k}_{\perp} & \cdots \\ -\alpha \mathbf{k}_{\perp} \cdot (\mathbf{k}_{\perp} + \mathbf{G}_{0,1}) & (\mathbf{k}_{\perp} + \mathbf{G}_{0,1})^2 & \cdots & -\alpha(\mathbf{k}_{\perp} + \mathbf{G}_{m,n}) \cdot (\mathbf{k}_{\perp} + \mathbf{G}_{0,1}) & \cdots \\ \cdots & \cdots & \cdots & \cdots & \cdots \\ -\alpha \mathbf{k}_{\perp} \cdot (\mathbf{k}_{\perp} + \mathbf{G}_{m,n}) & -\alpha(\mathbf{k}_{\perp} + \mathbf{G}_{0,1}) \cdot (\mathbf{k}_{\perp} + \mathbf{G}_{m,n}) & \cdots & (\mathbf{k}_{\perp} + \mathbf{G}_{m,n})^2 & \cdots \\ \cdots & \cdots & \cdots & \cdots & \cdots \end{vmatrix} \quad (36)$$

where $\alpha = \frac{2\pi a^2}{A}$. Note that unlike in the TM case, the coefficient α is independent of the eigenvalues κ .

The eigenvalues of the infinite matrix M can be calculated approximately as the eigenvalues of a truncated matrix with a finite rank. Thus, for $a/b \rightarrow 0$, we can explain the behavior of the lowest local band gap width for the TE modes at the X -points of square and triangular lattices.

Consider the lowest binary interaction of plane waves at the X -point. For the square lattice, the X -point corresponds to $\mathbf{k}_\perp = \frac{\pi}{b} \hat{\mathbf{e}}_x$. The two plane waves with the lowest $|\mathbf{k}_\perp + \mathbf{G}_{m,n}|$'s have $(m_1, n_1) = (0,0)$ and $(m_2, n_2) = (-1,0)$ and $|\mathbf{k}_\perp + \mathbf{G}_{m,n}| = \frac{\pi}{b}$. The truncated matrix M , describing the interaction of the two waves at the X -point, is

$$\tilde{M} = \begin{vmatrix} \left(\frac{\pi}{b}\right)^2 & \alpha \left(\frac{\pi}{b}\right)^2 \\ \alpha \left(\frac{\pi}{b}\right)^2 & \left(\frac{\pi}{b}\right)^2 \end{vmatrix}. \quad (37)$$

The eigenvalues of \tilde{M} are

$$\kappa_{1,2}^2 = \left(\frac{\pi}{b}\right)^2 (1 \pm \alpha). \quad (38)$$

For small a/b , the full width of the local band gap at the X -point scales as

$$\Delta\left(\frac{\omega b}{c}\right) = b(\kappa_2 - \kappa_1) = \pi\alpha = 2\left(\frac{\pi a}{b}\right)^2. \quad (39)$$

This agrees well with the numerical calculations using the PBGSS code⁸. Similarly, considering the interaction of the two lowest plane waves at the X -point of the triangular lattice ($\mathbf{k}_\perp = \frac{2\pi}{\sqrt{3}b} \hat{\mathbf{e}}_y$), we find that the full width of the local band gap at the X -point of the triangular lattice is given by

$$\Delta\left(\frac{\omega b}{c}\right) = \frac{2}{\sqrt{3}} \pi\alpha = \frac{8}{3} \left(\frac{\pi a}{b}\right)^2. \quad (40)$$

We calculate numerically the entire TE dispersion characteristics in both square and triangular lattices by including multiple plane-wave interactions at the metal rods. As illustrated in Figs. 3(b) and 4(b) for $a/b \rightarrow 0$, the approximation is good even for a small number of Fourier components. In Fig. 3(b), the results of the quasistatic calculations are shown with dots for the TE mode in a square lattice of rods with $a/b = 0.1$. Solid curves show the dispersion characteristics obtained from the PBGSS calculations⁸. Five to twelve of the lowest vectors in the reciprocal lattice (depending on the symmetry of the particular \mathbf{k} -point) are taken into account, and four lowest eigenmodes are plotted. Similarly, in Fig. 4 (b) the results of the

quasistatic calculations are shown with dots for the TE mode in a triangular lattice of rods with $a/b = 0.1$. Solid curves show the dispersion characteristics obtained from the PBGSS calculations⁸. Six to twelve of the lowest vectors of the reciprocal lattice were taken into account, and the four lowest eigenmodes are plotted. The three special points in Fig. 3(b), Γ , X, and M, correspond to $\mathbf{k}_\perp = 0$, $\mathbf{k}_\perp = \frac{\pi}{a}\hat{\mathbf{e}}_x$ and $\mathbf{k}_\perp = \frac{\pi}{a}(\hat{\mathbf{e}}_x + \hat{\mathbf{e}}_y)$, respectively. The three special points in Fig. 4(b), Γ , X, and J, correspond to $\mathbf{k}_\perp = 0$, $\mathbf{k}_\perp = \frac{2\pi}{\sqrt{3}a}\hat{\mathbf{e}}_y$ and $\mathbf{k}_\perp = \frac{2\pi}{3a}(\hat{\mathbf{e}}_x + \sqrt{3}\hat{\mathbf{e}}_y)$.

For the TE case, the agreement between the quasistatic and the PBGSS calculations is even better than for the TM case. This is because the interactions of the waves are determined by the small parameters $\alpha_{TE} = \frac{2\pi a^2}{A}$ (with $A \sim b^2$) for the TE case and $\alpha_{TM} = \frac{2\pi}{\ln(\kappa a)}$ (with $\kappa \sim 1/b$) for the TM case. For the same value of a/b , α_{TE} is much smaller than α_{TM} . Thus the quasistatic theory approximates the dispersion characteristics for the TE case much better than those for the TM case with the same value of a/b .

IV. CONCLUSIONS AND DISCUSSIONS

We have presented a self-consistent technique for calculating the dispersion characteristics in two-dimensional photonic band gap structures representing arrays of perfectly conducting rods. The technique is applicable for the structures with rod radius small compared to the distance between them and to the wavelength. First, we described the field in a periodic structure as a set of plane waves with wave numbers satisfying Bloch's theorem. Then we expressed self-consistently the induced current and charge distributions on the rods in terms of the electromagnetic wave field. We showed that these currents lead to the interaction between the plane waves in the structure, which is different for the TM and TE waves and affects the shape of the dispersion characteristics. Results were found in agreement with the dispersion characteristics previously calculated by the finite-difference PBGSS code⁸.

Although the effectiveness of the self-consistent quasistatic approach has been demonstrated only with ideal 2D metallic PBG structures, the technique may be generalized to treat 2D and 3D dielectric lattices and dielectric-metallic hybrids. This will be an important area for future investigations.

ACKNOWLEDGEMENTS

The authors wish to thank Prof. Michael Petelin (IAP RAS) for his inspiring ideas, and Dr. Michael Shapiro and Dr. Richard Temkin for useful discussions. We also thank Dr. Mark Hess for proofreading the manuscript. This research was supported in part by the Innovative Vacuum Electronics MURI Program, in part by the Department of Energy, High Energy Physics Division, and in part by Tech-X Corporation.

REFERENCES

1. E.Yablonovitch, T.J.Gmitter, and K.M.Leung, *Phys. Rev. Lett.* 67, 2295 (1991).
2. J.D.Joannopoulos, R.D.Meade, and J.N.Winn, *Photonic Crystals: Molding the Flow of Light* (Princeton Univ. Press, Princeton, 1995).
3. Y. Fink, D.J. Ripin, S. Fan, C. Chen, J.D. Joannopoulos, and E.L. Thomas, *J. of Lightwave Technology* 17, 2039 (1999).
4. D.R.Smith, S.Schultz, N.Kroll, M. Sigalas, K.M. Ho, and C.M. Soukoulis, *Appl. Phys. Lett.* 65, 645 (1994).
5. F.-R. Yang, K.-P. Ma, Y. Qian, and T. Itoh, *IEEE Trans. MTT* 48, 2092 (1999).
6. M.A. Shapiro, W.J. Brown, I. Mastovsky, J.R. Sirigiri, and R.J. Temkin, *Phys. Rev. Special Topics: Accelerators and Beams* 4, 042001 (2001).
7. J. R. Sirigiri, K.E. Kreischer, J. Machuzak, I. Mastovsky, M. A. Shapiro, and R. J. Temkin, *Phys. Rev. Lett.* 86, 5628 (2001).
8. E.I. Smirnova, C.Chen, M.A. Shapiro, J.R. Sirigiri, and R.J. Temkin, *J. Appl. Phys.* 91(3), 960 (2002).
9. N.A. Nicorovici, R.C. McPhedran, and L.C. Botten, *Phys. Rev. B*, 52(1), 1135 (1995).
10. T. Suzuki and P.K.L. Yu, *Phys. Rev. B* 57(4), 2229 (1998).
11. S.G. Johnson, P.R. Villeneuve, S.Fan, and J.D. Joannopoulos, *Phys. Rev. B* 62(12), 8212 (2000).
12. M. Qiu, S. He, *Phys. Rev. B* 61(19), 12871 (2000).
13. N.W. Ashcroft and N.D. Mermin, *Solid State Physics* (Holt, Rinehart and Winston, New York, 1976).
14. O. Madelung, *Introduction to Solid State Theory* (London, Springer, 1978).
15. L.D. Landau, E.M. Lifshitz, and L.P. Pitaevskii, *Electrodynamics of Continuous Media* (Pergamon Press, Oxford, 1984).

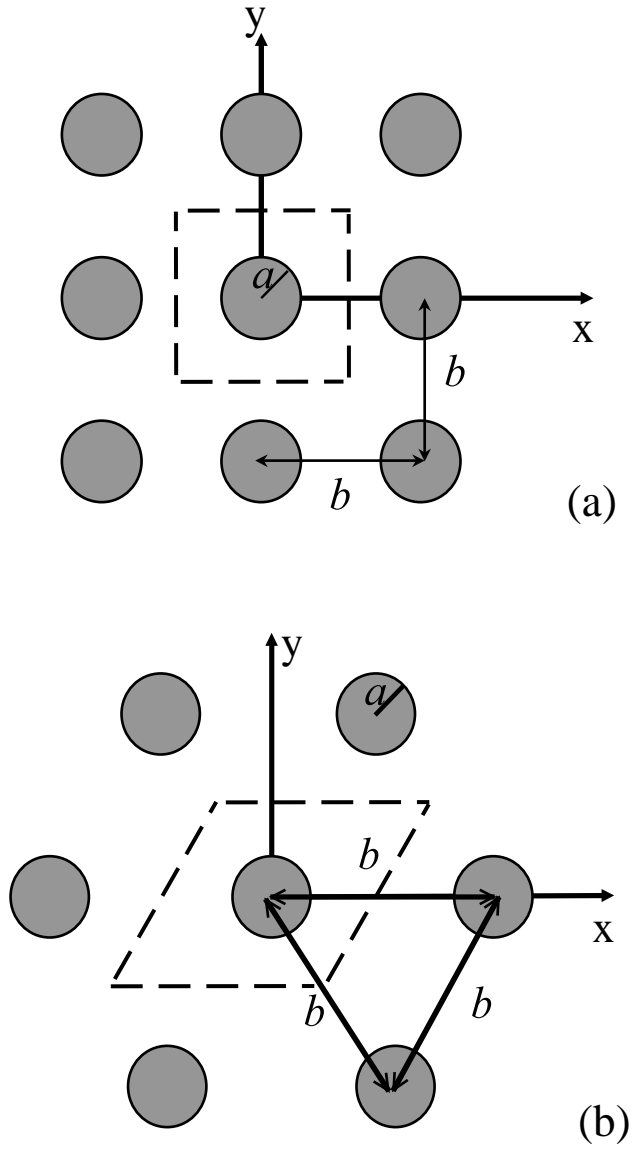


Fig. 1: Schematic of PBG structures representing (a) a square lattice and (b) a triangular lattice of perfectly conducting cylinders with radius a and spacing b .

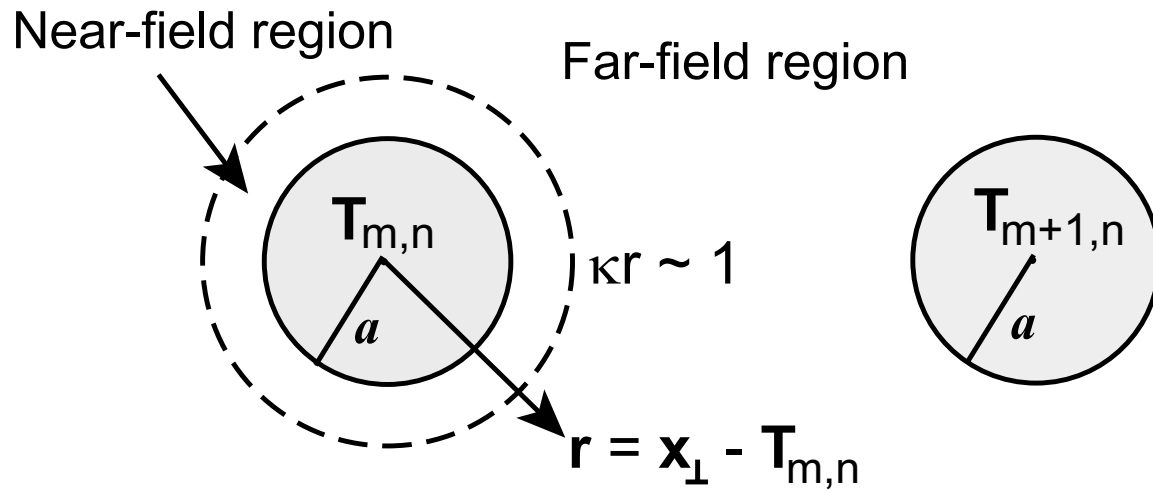


Fig. 2: Illustration of the near- and far-field regions in the quasistatic approximation.

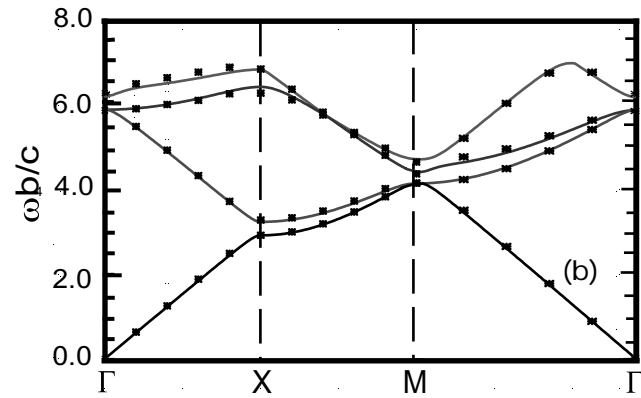
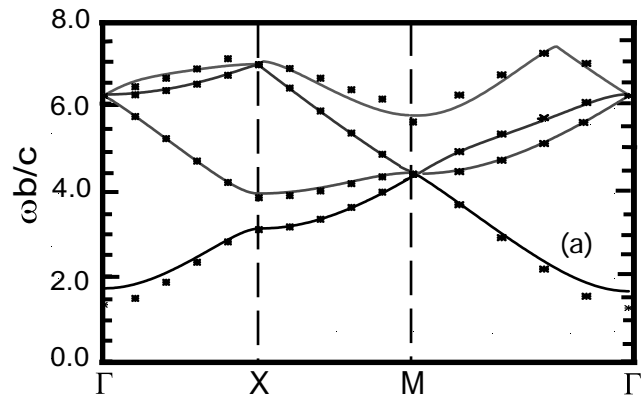


Fig. 3: Dispersion characteristics in the square lattice as calculated with the PBGSS code (solid curves) and the quasistatic approximation (dots) for (a) TM modes with $a/b = 0.05$ and (b) TE modes with $a/b = 0.1$.

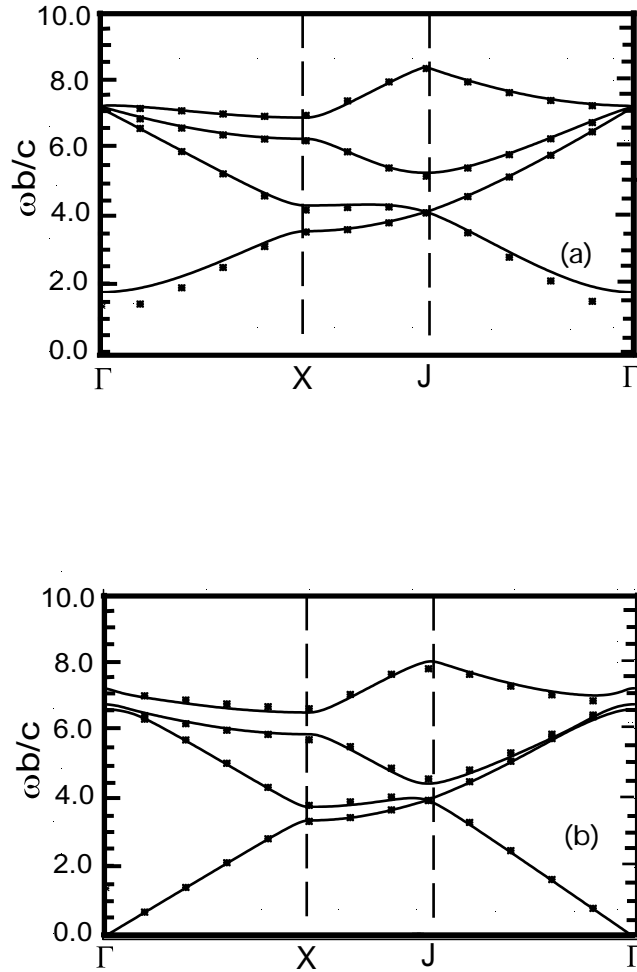


Fig. 4: Dispersion characteristics in the triangular lattice as calculated with the PBGSS code (solid curves) and the quasistatic approximation (dots) for (a) TM modes with $a/b = 0.05$ and (b) TE modes with $a/b = 0.1$.